Journal of Applied Polymer Science

Improved electrochemical performances of polyaniline by graphitized mesoporus carbon: Hybrid electrode for supercapacitor

Umashankar Male,[1] Palaniappan Srinivasan[1,2]

[1]Polymers & Functional Materials Division, CSIR-Indian Institute of Chemical Technology, Hyderabad 500007, India

[2]CSIR - Network Institutes for Solar Energy (NISE), New Delhi, India

Correspondence to: S. Palaniappan (E-mail: palani74@rediffmail.com)

ABSTRACT: In this work, graphitized mesoporus carbon (GMC) was used to increase the specific capacitance and cycle stability of polyaniline (PANI). Hybrid material of polyaniline-graphitized mesoporus carbon (GMCP) was prepared by *in situ* chemical polymerization of aniline in presence of sulphuric acid using ammonium persulfate oxidant with various amounts of GMC. Formation of hybrid sample was confirmed from X-ray diffraction, and the composite sample was stable up to 250°C. Morphology, crystalline nature, and electrochemical performance of GMCP were compared with that of its individual components, GMC and PANI. GMC showed particle morphology and PANI showed nanofiber morphology. GMCP2 composite showed nanofibrous form of PANI grown on GMC (spherical form) along with PANI nanofibers. Higher crystallinity was obtained for GMCP than that of PANI. Cycling stability of GMCP2 was carried up to 12,000 cycles at 1200 W kg^{-1} and the retention capacitance was 66% of its original capacitance of 243 F g^{-1}. With the same power density, GMC showed less capacitance value of 53 F g^{-1} with 92% retention and PANI showed capacitance of 187 F g^{-1} and it underwent 1500 cycles only. Higher supercapacitor performance was obtained for GMCP composite compared to that of its components, PANI and GMC. © 2015 Wiley Periodicals, Inc. J. Appl. Polym. Sci. **2015**, *132*, 42540.

KEYWORDS: applications; composites; conducting polymers; morphology; nanostructured polymers

Received 13 March 2015; accepted 26 May 2015

DOI: 10.1002/app.42540

INTRODUCTION

Supercapacitors have attracted considerable attention as an intermediate power source between conventional capacitors and rechargeable batteries. In general, there are two types of supercapacitors based on charge storage mechanisms: (1) Electrochemical double layer capacitor (EDLC), where capacitance is because of the formation of electrochemical double layer formed at the electrode/electrolyte interface and (2) Pseudocapacitor (PC), in which, the capacitance is because of redox reactions occurring in the bulk of the materials.[1–3] Carbon, conducting polymers and metal oxides are the active electrode materials used in supercapacitors. Carbon stores energy only at the interface, but metal oxides and conducting polymers exhibit both double-layer and faradaic capacitance (because of redox reactions) in energy storage. EDLCs provide very high power density compared to PCs, whereas PCs exhibits higher energy density than EDLCs. The carbon-based supercapacitor is the most advanced version of supercapacitors and is already on the market as high-performance devices with very long cycle life. Among the PC materials, metal oxides are generally expensive and toxic, whereas, the utilization and application of conducting polymers are limited by the relatively poor cycling stability owing to the damage of polymer backbone during the fast redox processes.

Recent research on energy storage systems, hybrid supercapacitor consists of higher power density EDLC component and high energy density PC component are being carried out.[4–20] In this work, we have selected graphitized mesoporous carbon (GMC) and polyaniline (PANI) for hybrid supercpacitor system. GMC is having large specific surface area and porosity. Among the conducting polymers, PANI is regarded as one of the most promising electrode materials because of high electrochemical activity, environmental stability, ease of synthesis, and low cost. Although few reports are available on the synthesis of mesoporus carbon PANI composites, they followed a two-step procedure wherein they synthesized mesoporus carbon using SBA-15[4–7] or F127[8–10] or P123[11,12] or colloidal silica[13] as templates and various organic materials as carbon precursors, the obtained mesoporus carbon was used in the subsequent synthesis of composite. In the present work, a simple one step method is followed wherein the commercially available GMC, wherein the conductivity of carbon is higher, to get a composite with better electrochemical performance.

Herein we report the synthesis of composite of PANI with GMC via *in situ* chemical oxidative polymerization of aniline in presence of GMC. Composite was characterized by X-ray diffraction (XRD), field emission scanning electron microscope (FESEM), transmission electron microscopy (TEM), and thermogravimetric analysis (TGA) analyses. Composite was used as electrode material in symmetric cell configuration. Electrochemical performances of composite were carried using cyclic voltammetry (CV), galvanostatic charge–discharge (CD) and electrochemical impedance (EIS) techniques.

Materials and Characterization

Aniline [S. D. Fine Chemicals, India], ammonium persulfate (APS), and sulfuric acid (H_2SO_4) [Rankem, India], graphitized mesoporus carbon (Sigma Aldrich, USA) were used as received. Freshly distilled aniline was employed in the reaction. All the reactions were carried out with distilled water and solvents.

EXPERIMENTAL

Preparation of Graphitized Mesoporus Carbon Polyaniline Composite (GMCP)

A series of GMCP samples were prepared using various amounts of GMC in the *in situ* polymerization of aniline via aqueous polymerization pathway. In a typical procedure, a known amount of GMC was dispersed in a 50 mL of aq. 1*M* H_2SO_4 solution containing 0.5 mL of aniline and sonicated till a uniform dispersion. Then, 1.44 g of APS pre-dissolved in 50 mL of aq. 1*M* H_2SO_4 solution was added to the above solution. The resulting reaction mixture was stirred for 4 h at ambient temperature. The reaction mixture was then filtered under vacuum, washed with an ample amount of distilled water and acetone until filtrate become colorless. The powder sample was dried at 50°C till a constant weight. The ratios (w/w) of aniline to GMC used were, 1 : 0.0025, 1 : 0.005, 1 : 0.01, 1 : 0.1, 1 : 0.2, 1 : 0.3, 1 : 0.4, and 1 : 0.5 and the corresponding GMCP composites are labeled as GMCP1, GMCP2, GMCP3, GMCP4, GMCP5, GMCP6, GMCP7, and GMCP8, respectively.

For comparison, PANI-sulfate salt was also prepared in the absence of GMC and labelled as PANI.

Preparation of Electrode and Supercapacitor Cell

The electrodes were fabricated by pressing the samples on stainless steel mesh (316 grade) (3 mg, 1 cm^2 area) by the application of 120 kg cm^{-2} of pressure without any additional binder. The electrochemical performances of the polymer samples were investigated using two-electrode system Swagelok type cells without a reference electrode. Two electrodes with identical sample were assembled into a supercapacitor with a cotton cloth separator in an electrolytic solution of aq. 1*M* H_2SO_4 solution.

Characterization

XRD profiles for the GMCP composite powders were obtained on a Bruker AXS D8 advance X-ray diffractometer (Karlsruhe, Germany) with Cu K_α radiation (land continuous) at a scan speed of 0.045° min^{-1}. Morphology studies of the polymer powder samples were carried out with a Hitachi S-4300 SE/N FESEM (Hitachi, Tokyo, Japan). Morphology studies of the polymer powder samples were carried out with a JEOL JSM-7600F (JEOL, USA) Field Emission Gun-Scanning Electron Microscope (FEG-SEM). The polymer powder sample was sputtered on a carbon disc with the help of double-sided adhesive tape. TEM measurement for GMCP2 was carried out with Philips CM200 instrument. TGA was performed with a TA Instruments TGA Q500 Universal at a heating rate of 10°C min^{-1} from room temperature to 700°C under nitrogen atmosphere. Cyclic voltammetry and galvanostatic charge–discharge experiments were carried out with a WMPG1000 multichannel potentiostat/galvanostat (Won-A-Tech, Gyeonggi-do, Korea). Cyclic voltammograms (CV) were recorded from −0.2 to 0.6 V at various sweep rates and charge–discharge experiments were carried out from 0 to 0.6 V at various current densities. Electrochemical impedance spectroscopy (EIS) measurement was performed with IM6ex (Zahner-Elektrik, Germany) by applying an AC voltage of 5 mV amplitude in the 40 kHz to 10 mHz frequency range at an applied voltage of 0.6 V using three-electrode cell configuration i.e., working electrode, platinum counter electrode, and calomel electrode as a reference electrode. All electrochemical measurements were carried out at ambient temperature.

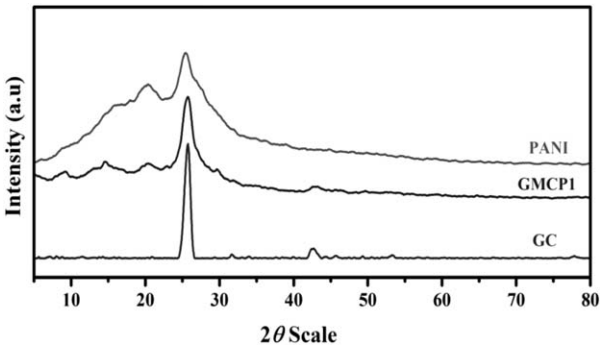

Figure 1. XRD patterns of GMC, PANI, and GMCP2.

RESULTS AND DISCUSSION

X-ray Diffraction

Figure 1 demonstrates the X-ray diffractograms of PANI, GMCP2, and GMC. XRD of GMC revealed an intense and sharp peak centred at $2\theta = 25.8°$, and a small broad peak centred at 42.4°. XRD pattern of GMC resembles the XRD of graphitic patterns of carbon.[21] XRD pattern of PANI showed one intense peak at 25.5° and a broad peak at 20.2° with two shoulder peaks at 14.7° and 8.7°. XRD patterns of GMCP showed peaks at 42.5°, 25.6°, 20°, 14.5°, and 8.9°. The first two peaks correspond to GMC and last four peaks correspond to PANI. A peak at 25.6° is because of GMC and PANI. All the peaks in GMCP2 are clear, which signpost the increase in the crystallinity of PANI.

Morphology Studies

FESEM images of GMC, GMCP2, and PANI are represented in Figure 2. FESEM of GMC shows particle morphology and PANI shows nanofiber morphology. FESEM image of GMCP2 composite shows nanofibrous form of PANI grown on GMC (spherical form) along with PANI nanofibers. The adsorbed aniline

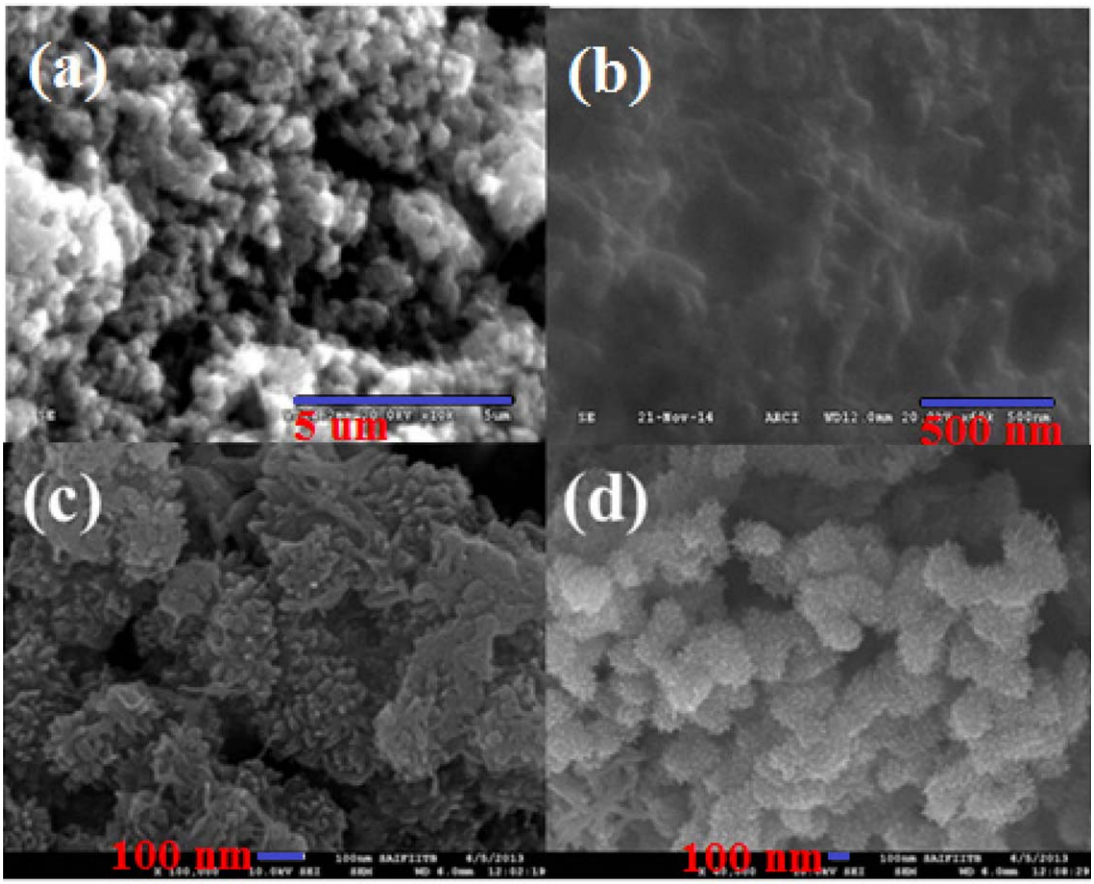

Figure 2. FESEM images (a) GMC, (b) PANI, and (c, d) GMCP2. [Color figure can be viewed in the online issue, which is available at wileyonlinelibrary.com.]

molecules act as nucleation sites and the polymerization took place preferentially and continuously near the adjacent GMC resulting in agglomerated particle like structures, further the enclosed GMC also provides the rigid support during the repetitive charge–discharge cycling of GMCP2 electrode. TEM picture of GMCP2 (Figure 3) clearly shows the formation of nanofibers of PANI on GMC and support the morphological observations made from FESEM [Figure 2(c, d)].

Thermogravimetry Analysis

Thermogravimetric thermograms of GMC, GMCP2, and PANI are shown in Figure 4. GMC is stable up to 590°C. Thermogram of GMCP2 is more or less similar to that of the thermogram of PANI. First step weight loss up to 110°C is because of loss of water molecules and the polymer is stable up to 250°C. Amount of water content present on GMC, GMCP2, and PANI materials are 0.1, 8.5, and 11 wt % respectively. The presence of

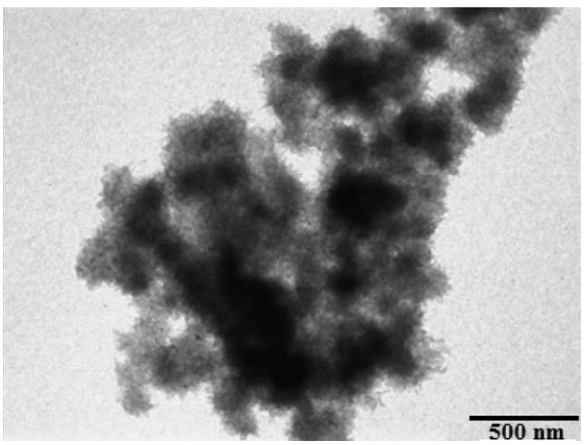

Figure 3. TEM image of GMCP2.

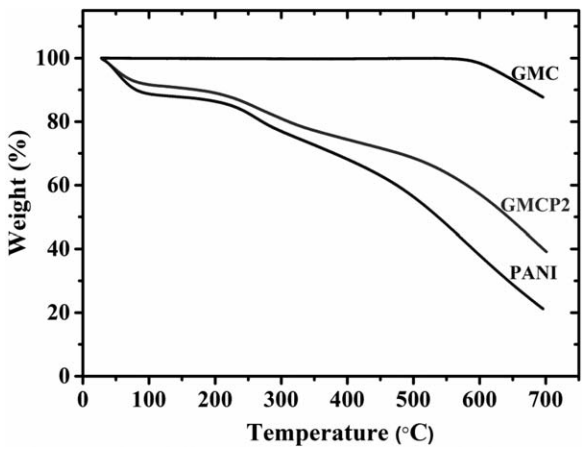

Figure 4. TG Thermograms of GMC, PANI and GMCP2.

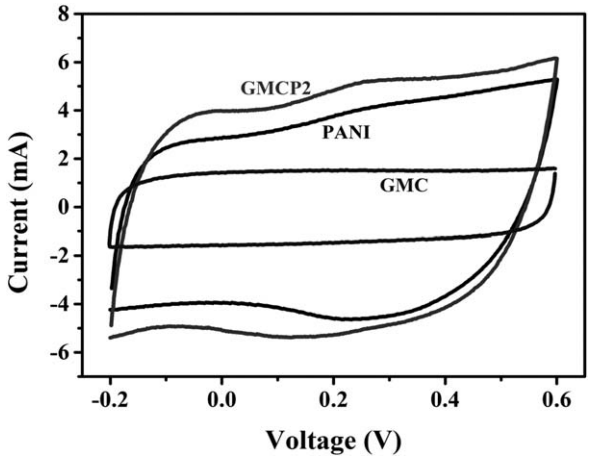

Figure 5. Cyclic voltammograms of GMCP2, PANI, and GMC at 10 mV s^{-1} in aq. 1*M* H_2SO_4.

water molecules in the electrode material will generally assist the ionic transportation in the electrolyte, thereby enhances the electrochemical performance.[14]

Cyclic Voltammetry Studies

Initially, electrochemical performance of GMCP composites were carried in a symmetric two electrode cell configurations in 1*M* H_2SO_4 electrolyte using cyclic voltammetric technique and the results are compared with that of its individual component, GMC and PANI. As a representative system, the cyclic voltammograms of GMCP2, PANI, and GMC are represented in Figure 5. The shape of the cyclic voltammograms is almost rectangular shape with good symmetry, indicates a rapid charging and discharging process, low internal resistance,[22,23] and excellent electrolyte accessibility throughout the electrode. Observation of small humps in the voltammograms of PANI and GMCP2 are because of the association of pseudo capacitive process (major) along with EDLC process (minor). The specific capacitance from CV curve (CV-C_s) was calculated according to the following equation:[14]

$$\text{CV}-C_s = \frac{Q}{\Delta V \cdot m}$$

where Q is the voltammetric charge, ΔV is the potential window, and m is the mass of the material in one electrode. The specific capacitance values for all the GMCP composites, PANI and GMC carried at various scan rates are represented in Figure 6. As can be seen from the figure that, the CV-C_s of PANI increase with the incorporation of GMC, attains a maximum, and then decreases. As a representative system, CV-C_s calculated at 1 mV s^{-1} of PANI is 366 F g^{-1}, increases with the addition of GMC and attains a maximum value of 533 F g^{-1} with the use of 0.5 wt % of GMC and then decreases to 345 F g^{-1} with 50 wt % of GMC. A similar trend was observed with higher scan rates, i.e., 2, 5, and 10 mV s^{-1} (Figure 2). The increase in CV-C_s with the addition of GMC (0.25 to 0.5 wt %) is expected to the well dispersion of GMC in GMCP composite their by facilitating the migration and diffusion of the electrolyte ions during the fast charge/discharge process and leading to effective utilization of electrode materials that contributes the total capacitance. Further increase of GMC (> 0.5 wt %), CV-C_s values decrease because of the incorporation of relatively less electrochemically active GMC compared to PANI in the GMCP composite material. Among the composites of GMCPs, GMCP2 showed higher CV-C_s value and hence further characterization was performed for GMCP2 composite.

The specific capacitance values of the optimized GMCP2 composite are 533, 519, 495, 404, 349, 318, 312, 312, and 311 F g^{-1}, at different scan rates of 1, 2, 5, 10, 20, 30, 40, 50, and 100 mV s^{-1}. The high specific capacitance of 311 F g^{-1} obtained even at a high scan rate of 100 mV s^{-1} represents the good rate capability of the electrode material. The decrease in specific capacitance with increasing scan rate may have been because of two reasons: (1) as the scan rate increased, it might have been difficult for the electric charge to occupy the available sites at electrode–electrolyte interface because of their limited range of migration and orientation in the electrolyte and (2) the *iR* of the supercapacitor.[24]

Charge–Discharge Studies

The galvanostatic charge/discharge (CD) experiments were carried at various current densities for GMCP2 and are shown in Figure 7. The shapes of all the CD curves are nearly linear and symmetric, which is the characteristic of a good capacitor. Slight deviation in the linear distribution of the charge–discharge

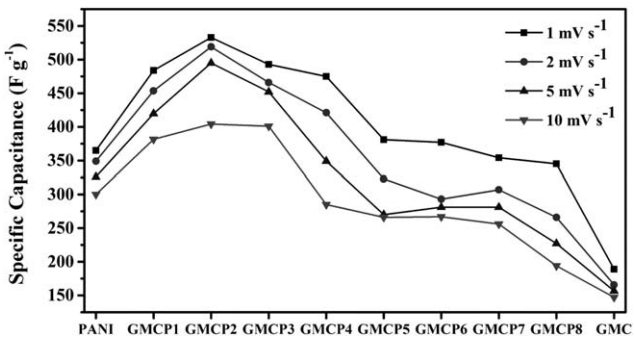

Figure 6. Behavior of specific capacitance at different scan rates for different GMCP composites along with its component, PANI and GMC.

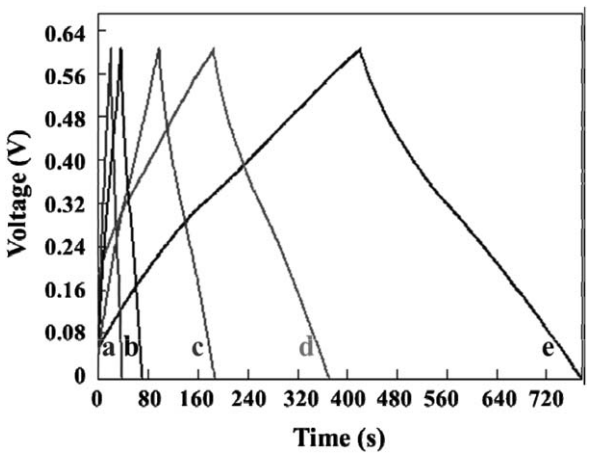

Figure 7. Galvanostatic charge–discharge curves of GMCP2 symmetric cell at (a) 4, (b) 2, (c) 0.8, (d) 0.4, and (e) 0.04 A g^{-1}.

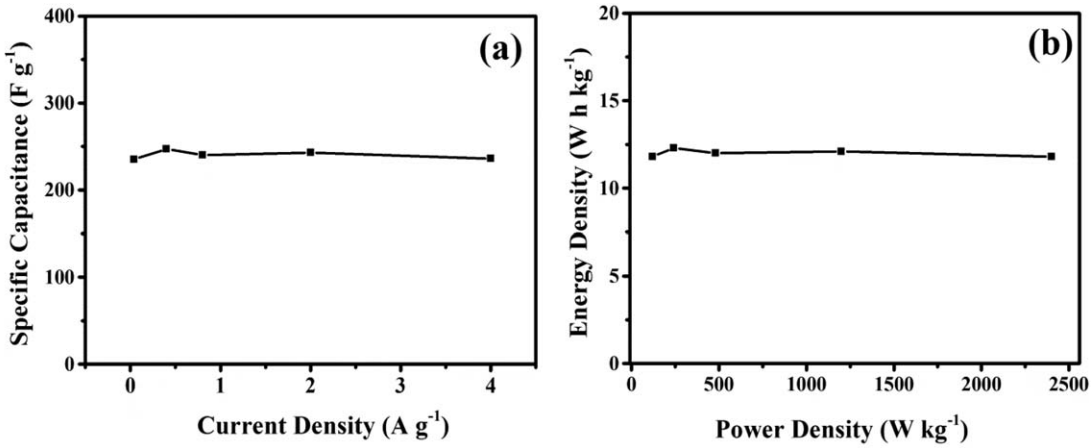

Figure 8. **(a)** Rate capability of GMCP2 at different current densities. **(b)** Ragone plot showing the variation of energy density of GMCP2 with power density.

curve is because of the pseudo capacitance, arising from the faradic reactions occurring in the polymer electrode.

The specific capacitance from charge–discharge curve (CD-C_s) of GMCP2 was calculated using the following equation,[12–14,25] CD-$C_s = (2 \times i \times \Delta t)(\Delta V \times m)^{-1}$, where i is the constant discharge current, Δt is the discharge time, ΔV is the voltage window during discharge, and m is the mass of the active material in one electrode. The factor of 2 comes from the fact that the total capacitance measured from the test cells is the addition of two equivalent single electrode capacitors in series. The rate capability of the GMCP2 electrode i.e., the behavior of specific capacitance with applied current density is shown in Figure 8(a). CD-C_s values are 236, 243, 240, 247, and 235 F g^{-1} at 4, 2, 0.8, 0.4, and 0.04 A g^{-1}, respectively. The observation of constant specific capacitance with charge–discharge rate is because of the uniform dispersion of GMC particles in the composite material, which enhances the electrochemical accessibility of electrolyte to the composite electrode through the loosely packed PANI nanofiber structures. Thus the composite can greatly reduce the diffusion length/resistance, resulting in the enhanced ion transport during the charge–discharge process even at higher current densities. This result signposts a good electrochemical capacitive characteristic of the composite material electrode. A similar observation was reported for the capacitor behavior of MWCNT/$NiCo_2O_4$ core/shell structures by Liu *et al.*[26]

The two important parameters for describing the behavior of the energy storage devices are energy density (E_d) and power density (P_d). A good electrode material is expected to provide high energy density and high capacitance simultaneously at high charge/discharge rates. Energy density is the energy stored per unit mass and was calculated by using the formulae[6,10,14,20] $E_d = 0.5 \cdot CD{-}C_s \cdot V^2$, whereas the Power density is the amount of energy delivered per unit mass and $P_d = E_d \cdot (t)^{-1}$, respectively. The energy densities of GMCP2 were 11.8, 12.3, 12, 12.1, and 11.8 W h kg^{-1} at power densities of 120, 240, 480, 1200, and 2400 W kg^{-1}, respectively. The Ragone plot demonstrating the variation of energy density with power density is shown in Figure 8(b). The result shows similar energy densities at various power densities signifying the good rate capability of the GMCP2 electrode. Similar energy densities are observed at various power densities and since the energy density is proportional to capacitance [almost constant capacitance was observed with various current densities in the charge–discharge behavior—Figure 8(a)].

Electrochemical Impedance Spectroscopy

Frequency dependent behavior of the GMC, PANI, and GMCP2 was carried from impedance analysis and the Nyquist plots are depicted in Figure 9. It consists of a single depressed semicircle in the high frequency region and a near vertical line in the low frequency region. Line in the low frequency region represents the characteristic feature of capacitive behavior. In the semicircle, the high frequency intercept on the real axis gives the solution resistance (R_s) of the materials. Values of R_s are the same for both GMC and PANI (0.6 Ω) and slightly higher for GMCP2 (1.4 Ω). The charge transfer resistance, R_{ct}, is associated with the charge transfer barriers within the system. The barriers here include the "electron transfer barrier" between the

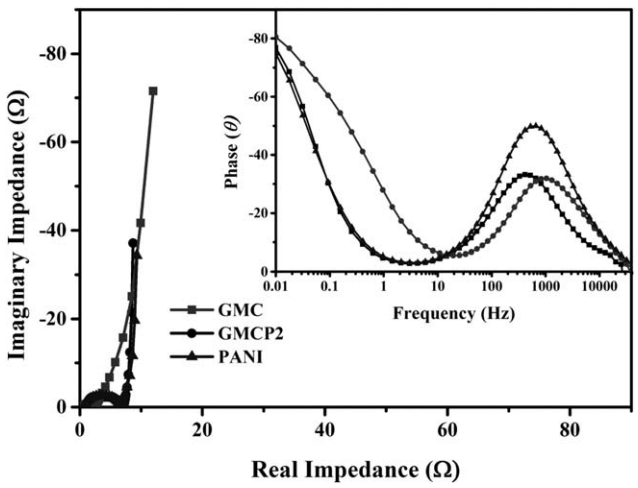

Figure 9. Nyquist plots (Inset: Bode plots) of GMC, PANI, and GMCP2 in the frequency range of 40 kHz to 10 mHz.

current collector and the capacitive material, and also the "ion transfer barrier" between the capacitive material and the electrolyte. In the impedance complex plane plot, R_{ct} can be derived from the diameter of the semicircle. The results infer that PANI (6.13 Ω) has the highest R_{ct} followed by GMCP2 (5.7 Ω) and GMC (2 Ω). The double layer capacitance for GMCP2, PANI, and GMC was calculated from the maximum of the semi-circle and is 84, 84, and 78 mF g^{-1} respectively.

The frequency at which is a deviation from the semicircle is the knee frequency,[27] which reflects the maximum frequency at which capacitive behavior is dominant. In other words, for a given capacitive material, the energy stored is not fully accessible at frequencies above the knee frequency.[28] The obtained knee frequency for GMC, PANI, and GMCP2 is 19.36, 4.27, and 3.02 Hz.

The specific capacitance from EIS measurement (EIS-*Cs*) of the electrode material was calculated using the following equation:[29]

$$EIS-Cs=\frac{-1}{2\pi^{*}f^{*}Z'^{*}m}$$

where f is the frequency at the tip of the spike (0.01 Hz), Z'' is the imaginary impedance at frequency f and m is the mass of the electroactive material. The specific capacitance is calculated based on above equation and is found to be 74, 154, and 172 F g^{-1} for GMC, PANI, and GMCP2, respectively. The operating frequency (the frequency at which the capacitance is 50% of its maximum value) of GMC is found to be 0.63 Hz corresponding to the characteristic relaxation time of 1.6 s, whereas the operating frequencies for PANI and GMCP is found to be same (1.77 Hz) with corresponding relaxation time of 0.6 s.

The impedance of an ideal capacitor with a zero real component is expressed by the following equation; $Z_c = Z' - Z''$, where Z_c, Z' and Z'' are the complex, real and imaginary impedance respectively. In the complex impedance plane (or the Nyquist plot), the above equation gives a straight line vertical to the Z′-axis. The phase angle, of an ideal capacitor is −90°. In reality, however, deviations are commonly observed as shown in the plots of phase angle vs logarithm of the applied frequency (inset in Figure 9). The phase angle observed in the present work for GMC, PANI, and GMCP2 is 80°, 75°, and 77°, respectively. Because $\tan\theta = Z'/Z''$ by definition, with Z' being frequency dependent, it is not surprising that θ can never reach 90°. The deviation from straight line at low frequencies has long been known for electrodes with inhomogeneity, porosity and/or other nonidealities.[29]

Cycle Life

Cycle life is an important parameter for the supercapacitors for practical applications. Thus the sample, GMCP2, was fabricated in two-electrode symmetric cell configuration and the cycle life was initially evaluated by performing 2000 CD cycles at two different current densities in aq. 1*M* H_2SO_4 electrolyte. After 2000 cycles, the capacitance remained at 82% and 77% of initial capacitance at 2 and 4 A g^{-1} respectively. Further, the cycling stability of GMCP2 was extended up to 12,000 cycles at 2 A g^{-1} and the retention capacitance was 66% (Figure 10). Decay in capacitance with cycle number is because of the repetitive volumetric expansion/contraction of PANI chains during the continuous injection/rejection (charge/discharge) of electrolyte ions, deteriorating the charge distribution and conformation of π conjugated PANI chains. As can be seen from Figure 10, the plot of cycle life of GMCP2 is not smooth and this may be because of variation in injection and rejection kinetics of ions into the electrodes. For comparison, cycle life studies are also performed on GMC and PANI electrode materials in two-electrode cell configurations at 2 A g^{-1} (Figure 10). The GMC showed an initial capacitance of 53 F g^{-1} and is maintained almost constant for 12,000 cycles (92% retention); whereas PANI showed an initial capacitance of 187 F g^{-1} and it withstood 1500 cycles only.

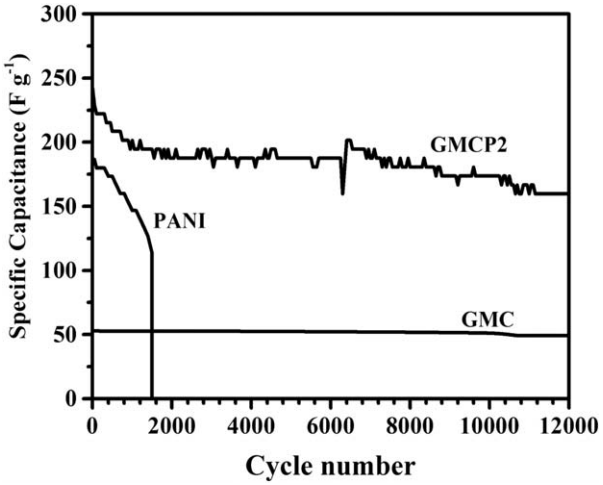

Figure 10. Specific capacitance with cycle numbers for GMC, PANI, and GMCP2 at 2 A g^{-1}.

CONCLUSIONS

Specific capacitance of PANI was increased to 533 F g^{-1} with the use of 0.5 wt % of graphitized mesoporous carbon. Hybrid material was prepared via *in situ* polymerization of aniline in presence of graphitized mesoporous carbon. Thermal stability of the composite was 250°C. The specific capacitance, energy, and power densities of the composite material was 236 F g^{-1}, 11.8 W h k g^{-1}, and 2400 W k g^{-1}, respectively, even at a high discharge current density of 4 A g^{-1}. About 12,000 charge–discharge cycles were carried at 2 A g^{-1} and it retained 66% of its original capacitance. The energy densities of the composite were 11.8, 12.3, 12, 12.1, and 11.8 W h kg^{-1} and independent at power densities of 120, 240, 480, 1200, and 2400 W kg^{-1} respectively. Composite was obtained with a knee frequency (3 Hz), operating frequency (1.8 Hz) with relaxation time of 0.6 s.

ACKNOWLEDGMENTS

The authors thank CSIR, New Delhi under the TAPSUN program (NWP-0056) for funding. We are thankful to Dr. M. Lakshmi Kantam, Director and Dr. K.V.S.N. Raju, CSIR-IICT for their support and encouragement. Umashankar Male is thankful to CSIR, India for financial assistance.

REFERENCES

1. Zhang, Y.; Feng, H.; Wu, X.; Wang, L.; Zhang, A.; Xia, T.; Dong, H.; Li, X.; Zhang, L. *Int. J. Hydrogen Energy* **2009**, *34*, 4889.
2. Wang, G.; Zhang, L.; Zhang, J. *Chem. Soc. Rev.* **2012**, *41*, 797.
3. Snook, G. A.; Kao, P.; Best, A. S. *J. Power Sources* **2011**, *196*, 1.
4. Wang, Y.-G.; Li, H.-Q.; Xia, Y.-Y. *Adv. Mater.* **2006**, *18*, 2619.
5. Cai, J. J.; Kong, L. B.; Zhang, J.; Luo, Y. C.; Kang, L. *Chin. Chem. Lett.* **2010**, *21*, 1509.
6. Zhang, Z.; Wang, G.; Li, Y.; Zhang, X.; Qiao, N.; Wang, J.; Zhou, J.; Liu, Z.; Hao, Z. *J. Mater. Chem. A* **2014**, *2*, 16715.
7. Yan, Y.; Cheng, Q.; Wang, G.; Li, C. *J. Power Sources* **2011**, *196*, 7835.
8. Xing, W.; Yuan, X.; Zhuo, S.-P.; Huang, C.-C. *Polym. Adv. Technol.* **2009**, *20*, 1179.
9. Zhou, S.; Mo, S.; Zou, W.; Jiang, F.; Zhou, T.; Yuan, D. *Synth. Met.* **2011**, *161*, 1623.
10. Yan, Y.; Cheng, Q.; Zhu, Z.; Pavlinek, V.; Saha, P.; Li, C. *J. Power Sources* **2013**, *240*, 544.
11. Bulusheva, L. G.; Fedorovskaya, E. O.; Okotrub, A. V.; Maximovskiy, E. A.; Vyalikh, D. V.; Chen, X.; Song, H. *Phys. Status Solidi B* **2011**, *248*, 2484.
12. Li, L.; Song, H.; Zhang, Q.; Yao, J.; Chen, X. *J. Power Sources* **2009**, *187*, 268.
13. Zhang, L.; Li, S.; Zhang, J.; Guo, P.; Zheng, J.; Zhao, X. *Chem. Mater.* **2010**, *22*, 1195.
14. Uppugalla, S.; Male, U.; Srinivasan, P. *Electrochim. Acta* **2014**, *146*, 242.
15. Park, S.; Yoo, Y. G.; Nam, I.; Bae, S.; and Yi, J. *Energy Technol.* **2014**, *2*, 677.
16. Xiong, G.; Meng, C.; Reifenberger, R. G.; Irazoqui, P. P.; Fisher, T. S. *Adv. Energy Mater.* **2014**, *4*, n/a.
17. Li, L.; Qiu, J. J.; Wang, S. R. *Soft Matter* **2013**, *11*, 503.
18. Li, L.; Qiu, J. J.; Wang, S. R. *Electrochim. Acta* **2013**, *99*, 278.
19. Li, L.; Zhang, X.; Qiu, J. J.; Weeks, B. L.; Wang, S. R. *Nano Energy* **2013**, *2*, 628.
20. Li, L.; Wang, S.; Hui, D.; Qiu, J. *Compos. B Eng.* **2015**, *71*, 40.
21. Park, S.; An, J.; Potts, J. R.; Velamakanni, A.; Murali, S.; Ruoff, R. S. *Carbon* **2011**, *49*, 3019.
22. Wang, Y.; Shi, Z.; Huang, Y.; Ma, Y.; Wang, C.; Chen, M.; Chen, Y. *J. Phys. Chem. C* **2009**, *113*, 13103.
23. Chunsheng, D.; Jeff, W. Y.; Ning, P. *Nanotechnology* **2005**, *16*, 350.
24. Sivaraman, P.; Rath, S. K.; Hande, V. R.; Thakur, A. P.; Patri, M.; Samui, A. B. *Synth. Met.* **2006**, *156*, 1057.
25. Wang, X.; Wang, X.; Liu, L.; Yi, L.; Hu, C.; Zhang, X.; Yi, W. *Synth. Met.* **2011**, *161*, 1725.
26. Liu, W.; Lu, C.; Liang, K.; Tay, K. B. *J. Mater. Chem. A* **2014**, *2*, 5100.
27. Dandekar, M. S.; Arabale, G.; Vijayamohanan, K. *J. Power Sources* **2005**, *141*, 198.
28. Hughes, M.; Chen, G. Z.; Shaffer, M. S. P.; Fray, D. J.; Windle, A. H. *Chem. Mater.* **2002**, *14*, 1610.
29. Zhang, S.; Peng, C.; Ng, K. C.; Chen, G. Z. *Electrochim. Acta* **2010**, *55*, 7447.